ADVANCED FUNCTIONAL MATERIALS

The Relationship Between Nanoscale Structure and Electrochemical Properties of Vanadium Oxide Nanorolls**

By *Dong Sun*, *Chai Won Kwon*, *George Baure*, *Erik Richman*, *Jenifer MacLean*, *Bruce Dunn*,* and *Sarah H. Tolbert**

In this paper, we explore the relationship between the nanoscale structure and electrochemical performance of nanoscale scrolls of vanadium oxides (vanadium oxide nanorolls). The vanadium oxide nanorolls, which are synthesized through a ligand-assisted templating method, exhibit different morphologies and properties depending upon the synthetic conditions. Under highly reducing conditions, nearly perfect scrolls can be produced which have essentially no cracks in the walls (well-ordered nanorolls). If the materials are produced under less reducing conditions, nanorolls with many cracks in the oxide walls can be generated (defect-rich nanorolls). Both types of samples were examined by X-ray diffraction (XRD), transmission electron microscopy (TEM), and X-ray photoemission spectroscopy (XPS) to characterize their local structure, local redox state, and nanoscale structure. After ion-exchange to replace the templating ammonium ions with Na^+, the ability of these materials to electrochemically intercalate lithium reversibly was investigated. In sweep voltammetry experiments, the well-ordered nanorolls showed responses similar to those seen in crystalline orthorhombic V_2O_5. In contrast, the defect-rich vanadium oxide nanorolls behaved electrochemically more like sol–gel-prepared vanadium oxide materials. Moreover, the specific capacity of the well-ordered nanorolls was about 240 mA h g^{-1} while that of the defect rich nanorolls was found to be as much as 340 mA h g^{-1} under these same conditions. Disorders on both the atomic and nanometer length scales are believed to contribute to this difference.

1. Introduction

There is a growing body of experimental evidence which indicates that nanodimensional materials for lithium secondary batteries possess improved electrochemical properties as compared to their bulk counterparts.[1] Among the properties reported are enhanced reactivity towards lithium,[2,3] suppression of phase transformations to obtain electrochemical reversibility,[4] and the use of defects and high surface area to produce high capacity for lithium.[5–7] In addition, the short diffusion lengths in nanodimensional materials are also beneficial for electrode kinetics.

Recently, Nesper and co-workers reported a novel nanostructured material.[8–10] By employing the ligand-assisted templating method developed for the synthesis of periodic nanoporous metal oxides,[11–14] they were able to synthesize vanadium oxide with a nanoscale scroll-like structure. The morphology of this material suggests that it might be attractive for lithium battery electrodes because it combines the basic geometry of bulk layered vanadium oxide with unique features that arise from its nanoscale structure. These features include a large exterior surface area and a potentially more accessible interior surface area. In addition, the structures are intrinsically anisotropic in that the roll axis is very different from the cross-sectional direction; it may be possible to exploit this anisotropy in some applications.

The electrochemical properties of pristine vanadium oxide nanorolls as well as alkali or alkaline earth cation exchanged nanorolls have been examined by several research groups.[8,15–18] Their results indicate that ion-exchanged versions of this unique nanostructured vanadium oxide may be promising for rechargeable lithium battery applications. However, limited capacity for lithium and variable capacity upon cycling raise some questions regarding the advantage of these materials over bulk layered vanadates or sol–gel prepared vanadates.

In our laboratories, we have been exploring the possibility of increasing the specific capacity of vanadium oxide nanorolls as reversible electrode material for rechargeable lithium batteries without compromising their novel nanoroll structure. Nanoscale vanadium oxide materials prepared via sol–gel chemistry have demonstrated significant improvements in electrochemical properties and it is interesting to consider whether vanadium oxide nanorolls can exhibit similar improvements.[5–7] Here we report our results on the relationship between the specific capacities for lithium and the nanoscale structures of these vanadia nanorolls. We find that defect-rich vanadium oxide nanorolls show a significant increase in specific capacity com-

[*] Prof. S. H. Tolbert, Dr. D. Sun, E. Richman, J. MacLean
Department of Chemistry and Biochemistry
University of California Los Angeles
Los Angeles, CA 90095 (USA)
E-mail: Tolbert@chem.ucla.edu
Prof. B. Dunn, Dr. C. W. Kwon, G. Baure
Department of Materials Science and Engineering
University of California Los Angeles
Los Angeles, CA 90095 (USA)
E-mail: BDunn@ucla.edu

[**] We thank Dr. Prikhodko in the Material Science and Engineering Department at UCLA for assistance with TEM. This work is supported by the Office of Naval Research through MURI grant N00014-01-1-0757. SHT is an Alfred P. Sloan Foundation research fellow.

 DOI: 10.1002/adfm.200400056

pared to those without defects in their wall structures. We relate this high capacity to the V^{4+}/V^{5+} ratio in the nanoroll composite, to cracks in the wall, and to residual organic surfactant that remains in the nanorolls during cycling.

2. Results and Discussion

2.1. Synthesis and Characterization of Surfactant/Vanadia Composite Nanorolls

Transition metal oxides, such as vanadium, iron, cobalt, and manganese, have been studied extensively as cathode materials for rocking-chair rechargeable lithium batteries over the last several decades.[19,20] Most of these materials consist of layered or channeled structures which allow lithium ions to reversibly intercalate or deintercalate, compensated by changes in redox state of the transition metal ion. Recently, there have been efforts to expand the search for better performance cathode materials by moving into the nanoscale regime.[1,2,4,6,21] Compared to bulk crystalline or amorphous transition metal oxides, the nanostructured oxides possess short lithium ion diffusion paths and often have high surface areas. Vanadium oxide nanorolls, as discussed by Nesper and co-workers, have the potential to benefit from these same phenomena.[16,22] We will demonstrate, however, that electrochemical performance depends not only on size scale, but also correlates with the details of nanoscale morphology, wall structures, and composite composition.

We have found that the degree of order in a sample of vanadium oxide nanorolls can be tuned by varying the amount of reducing agent present during hydrothermal treatment. When the amount of reducing agent is decreased from the optimal concentration, defected nanorolls are produced. Transmission electron microscopy (TEM) images of these nanorolls (Fig. 1) reveal the basic structural differences between the well-ordered and defect-rich materials. Figure 1 (top) shows TEM images of well-ordered and defect-rich nanorolls, respectively, at low magnification. In these images, the gross morphology of the nanorolls is easily seen. The well-ordered nanorolls can be several micrometers in length and several hundred nanometers in diameter. When magnified, these well-ordered nanorolls show an almost perfect wall structure without any cracks in the walls (Fig. 1, bottom left). The number of layers ranges from just a few up to more than ten. The distance between the layers is roughly 3.0 nm. By contrast, the nanorolls produced with lower relative concentration of reducing agent show very rough surfaces (Fig. 1, top right). When examined at high resolution, many cracks in the wall are easily observed (Fig. 1, bottom right). These cracks play an important role in the electrochemical properties of these nanorolls, which will be discussed later.

In Figure 2, we show the low-angle XRD patterns of three samples: the orange-red vanadium/surfactant composite ob-

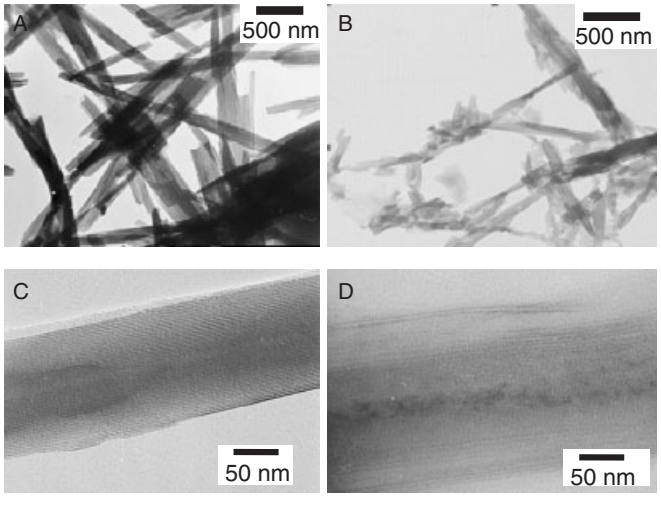

Figure 1. TEM images of well-ordered (left (A,C)) and defect-rich (right (B,D)) vanadium oxide nanorolls. Top: low resolution images; bottom: high resolution images. In both cases, the defect-rich nanorolls show rough surfaces, cracks, and regions where the layers are not perfectly stacked. By contrast, the well-ordered nanorolls show straight surfaces, no cracks, and near-perfect layer spacings.

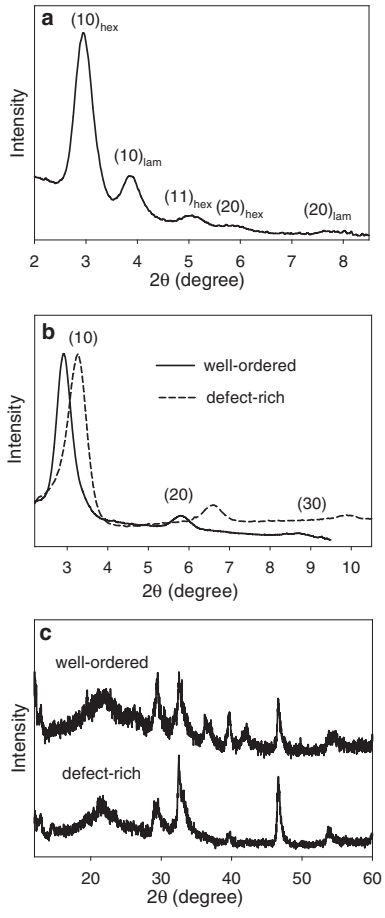

Figure 2. X-ray diffraction data from various vanadia nanoroll materials. Low-angle XRD patterns of the nanostructured vanadium oxide composite before hydrothermal treatment (a) indicates a mixture of hexagonal honeycomb and lamellar morphologies. After hydrothermal treatment (b) layered vanadium oxide nanorolls are produced. Both well-ordered and defect-rich materials show a simple layered structure, although the layer spacing is slightly different. High-angle XRD of well-ordered and defect-rich vanadia nanorolls (c) also indicates structural differences on the atomic scale. All 2θ data are presented relative to Cu Kα radiation.

ADVANCED FUNCTIONAL MATERIALS

tained before hydrothermal treatment (a), and well-ordered and defect-rich vanadia nanorolls, both obtained after hydrothermal treatment (b). The vanadium oxide/surfactant composite obtained before hydrothermal treatment (Fig. 2a) shows five observable peaks. Three of these peaks show a $1:\sqrt{3}:2$ position ratio and thus can be indexed as the (10), (11), and (20) peaks of a *p*6mm two-dimensional (2D) hexagonal honeycomb geometry with a lattice constant a of ~3.5 nm. The other two peaks can be indexed as (10) and (20) of a simple lamellar structure with a layer spacing ~2.3 nm.

After hydrothermal treatments at 180 °C, the hexagonal phase disappears and both the well-ordered and defect-rich nanorolls show only a layered lamellar structure, as seen in Figure 2b. However the layer spacing is slightly different between the two materials, with the well-ordered nanorolls having a larger spacing than the defect-rich material (3.0 nm vs. 2.7 nm). This difference can be accounted for by different amounts of surfactant molecules trapped between the vanadium oxide layers. The amount of these surfactant molecules was studied by elemental analysis (shown in Table 1). The data indicates that in the well-ordered nanorolls, there is substantially more surfactant. These surfactant molecules serve as pillars between the layers with the long alkyl chains extended between the vanadium oxide surfaces. With more surfactant molecules present, the long tails of the surfactant molecules have less freedom to "wiggle", which results in a more rigid alkyl chain conformation with the chains almost perpendicular to the vanadia layer. This produces a slightly larger layer spacing. By contrast, when less surfactant is present, the chains can tilt or bend, producing a smaller layer spacing.

Table 1. Surfactant and V^{4+} content in well-ordered and defect-rich nanorolls, both before and after Na^+ ion-exchange (30 min exchange time).

Sample	Surfactant content [mmol g^{-1}]	V^{4+} [mole-%]
well-ordered nanorolls	2.23	45
defect-rich nanorolls	1.83	24
Na-exchanged, well-ordered nanorolls	0.363	–
Na-exchanged, defect-rich nanorolls	0.326	–

The structural differences between the well-ordered and defect-rich vanadium oxide nanorolls at the atomic scale can also be seen in high-angle XRD. High-angle XRD data obtained on both the well-ordered and defect-rich nanorolls are shown in Figure 2c. The XRD patterns of these nanorolls are similar to those reported previously, with several low intensity peaks observed at higher 2θ.[18,23] These peaks have been indexed to a 2D square lattice with a ~0.61 nm.[18,23] However, some differences are noticeable between these two samples. In the 2θ range between 35° and 45°, there are three very weak peaks observable in the case of well-ordered nanorolls; one of these peaks has been assigned to the (220) reflection.[23] These three peaks are almost undetectable in the defect-rich nanorolls. This is an indication that the crystal structures of the walls and the registry of the layers are slightly lower in the defect-rich material.

The fundamental cause of all of these differences can be related to atomic-scale chemistry by examining the ratios of V^{4+}/V^{5+} in the oxide walls using XPS, as shown in Figure 3 and Table 1. From the XPS analysis, there is about 45 % V^{4+} in the well-ordered nanorolls (V^{4+} to V^{5+} ratio is ~1:1.2), which is in excellent agreement with reported data,[23,24] but only 24 % V^{4+} in the defect-rich composites (V^{4+} to V^{5+} ratio is ~1:3.2). These differences relate simply to the experimental conditions used during synthesis. In the hydrothermal treatment, 2-propanol is added as the reductant. During the treatment, the hydroxyl group on 2-propanol is oxidized by V^{5+} to a ketone in the presence of water. The relative amount of 2-propanol added thus controls the ratio of V^{4+}/V^{5+} in the final material. The smaller the amount of 2-propanol, the lower the V^{4+}/V^{5+} ratio.

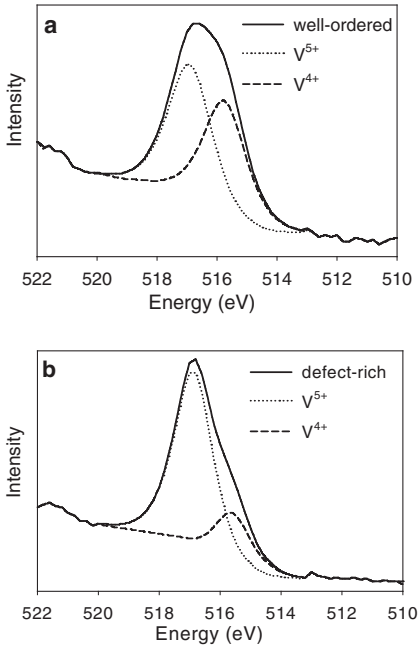

Figure 3. XPS data obtained on a) well-ordered and b) defect-rich vanadia nanorolls. The peak at 516.9 eV is assigned to the V^{5+} $2p_{3/2}$ orbital and that at 515.7 eV to the V^{4+} $2p_{3/2}$ orbital. In the well-ordered nanorolls, V^{4+} constitutes 45 % of the total vanadium while in defect-rich nanorolls, only 24 % of the vanadium is in the form of V^{4+}. In the vanadia structure, V^{4+} ions lead to anion sites in the walls, while V^{5+} produces the neutral oxide. The surfactant template associates with the anion sites.

The difference in V^{4+}/V^{5+} ratio plays an important role in the formation of the nanoscale structure of the vanadia rolls and in determining the local crystal structure of the vanadium oxide walls. The tube walls are composed of vanadium oxo-anions and thus carry a neutral or negative charge. V^{5+} effectively neutralizes this charge, while V^{4+} does not. As a result, the total anionic charge density on the inorganic wall is a direct function of the V^{4+} content. The higher the anionic charge on the wall, the larger the amount of cationic surfactant that can be asso-

ciated with the composite. We note that the electrostatic interaction between the anionic V^{4+} sites and the cationic ammonium surfactants is much stronger than dative bonding between neutral V^{5+} sites and neutral amine head group.

The formation of a nanoroll structure with vanadium oxide, as well as other nanostructures prepared via 'wet chemistry' using surfactants as structural directing agents, is a complicated process. In surfactant templated syntheses of nanostructured transition metal oxides, the van der Waals' interaction between the surfactant tails, the electrostatic interactions between the inorganic and organic components, and the polymerization of the transition metal oxide together control the final nanoscale structure of the composites.[25] The vanadium oxide composite produced before hydrothermal treatment exhibits a mixture of nanoscale architectures (Fig. 2a), which is an indication of the exquisite balance between the forces involved in the formation of these nanostructures. During the hydrothermal treatment step, several structural rearrangements occur. The hexagonally ordered structure must first transform into a lamellar structure. The transformation likely results from a combination of two effects. The first is the reduction of V^{5+} to V^{4+}, which helps drive the composite toward a lower curvature structure by increasing the inorganic charge density.[26] The second is an increase in the thermal motion of the surfactant tails, which also helps drive the formation of a lower curvature lamellar phase.[27] Both of these effects have been observed previously to control hexagonal-to-lamellar phase transitions in surfactant templated silica based materials.[27–30]

The many-layered lamellar structure then has to exfoliate into a single layer or few-layered stacks in order to roll up into a nanoroll structure. The activation barriers of these transformations have not been studied yet, but we suspect that the activation barrier for the hexagonal-to-lamellar phase transformation or for exfoliating the bulk layered structure is probably rate determining. In the more rapid rolling-up process that follows, the higher the surfactant content, the stronger the hydrophobic interactions and thus the more ordered the final material. With insufficient surfactant electrostatically associated with the layers, the overall vanadia hydrophobicity should be lower, and thus the driving force for rolling should be lower. As a result of these weaker interactions, the vanadia layers are held together less strongly and a less ordered, cracked composite results.

2.2. Ion Exchange to Form Alkali Containing Nanorolls

The as-synthesized vanadium oxide nanorolls with surfactant molecules trapped inside show poor performance for rechargeable battery applications. Their voltammetric and charge-discharge behavior degrades rapidly upon cycling.[9] It has been observed, however, that replacing the organic ammonium with alkali or alkali earth cations improves their electrochemical performance dramatically.[17,18] In the research reported here, we chose to ion-exchange our nanoroll samples with sodium hexafluorophosphate under ambient temperature in ethanol and water mixed solvents. The high solubility of both the surfactant and the sodium hexafluorophosphate in ethanol facilitates the exchange of ions in the nanostructure. The ion-exchange process was monitored by XRD and TEM. We find that if less than a threefold excess of sodium hexafluorophosphate is used in the solution (mole ratio relative to the amount of protonated surfactant in the nanorolls), there is no change in layer spacing observable from low-angle X-ray diffraction studies. This does not, however, mean there is no exchange occurring, because the layer spacing is controlled by the longest surfactant molecules that are oriented perpendicularly to the vanadium oxide surface. As long as there are enough surfactant molecules contained between the walls to serve as pillars, the layer spacing of the nanorolls should not change significantly. With more than three equivalents of sodium ions used in the ion-exchange, the layer spacing changes within a few minutes.

Figure 4a shows X-ray diffraction patterns of the ion-exchanged well-ordered and defect-rich nanorolls. A fundamental diffraction peak which corresponds to the layer spacing is

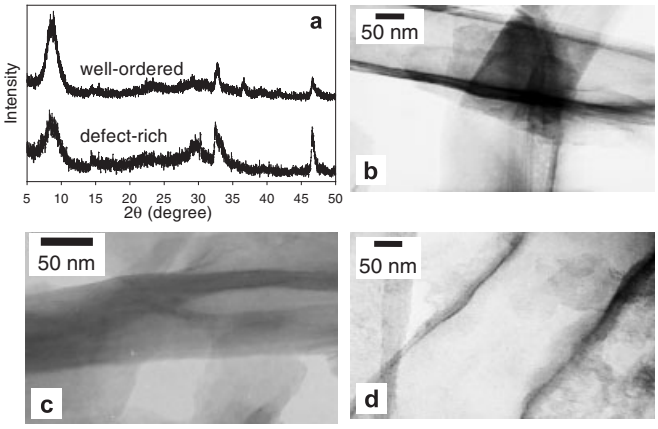

Figure 4. Structural data obtained on Na-exchanged vanadia nanorolls. XRD of well-ordered and defect-rich vanadium oxide nanorolls after 30 min ion-exchange time (a) shows that the fundamental peak position and thus the layer spacing has decreased. The layer spacing is now the same for both samples. A TEM image of the well-ordered nanorolls after sodium ion exchange (b) similarly shows a decrease in layer spacing. This same decrease in seen in defect-rich materials (c) although there appears to be more exfoliated layers in this sample. The nanoroll structure is retained upon electrochemical cycling, as seen in part (d) which shows a TEM image of well-ordered sodium ion-exchanged nanorolls after electrochemical charge–discharge cycling.

observed at low angle for both samples. From this peak, we can deduce that the layer spacing decreases from 3.0 nm and 2.7 nm to ~1.0 nm, roughly the same for both of the nanoroll samples. The other less intense peaks are from the local crystal structure of the vanadium oxide wall, which are the same as the nanorolls before the ion-exchange. Since there is no redox reaction involved in the ion-exchange process, we do not expect the V^{4+}/V^{5+} ratio to be changed during this process.

TEM images of well-ordered Na-exchanged nanorolls are shown in Figures 4b. The image indicates that the basic nanoroll structure is preserved upon ion exchange, but that the inner empty space of the nanorolls is significantly enlarged, sug-

ADVANCED FUNCTIONAL MATERIALS

gesting some "unrolling" upon ion-exchange. Due to resolution limitation with our TEM, it is difficult to explicitly see the layer separation, which is slightly less than 1 nm. Based on the total wall thickness, however, we believe that the number of layers in the walls is reduced to fewer than five layers for the majority of the samples, again consistent with some "unrolling". Similar data is obtained for defect-rich nanorolls (Fig. 4c), although in this case, it appears that there are some unrolled layers present in the TEM image.

After sodium ion-exchange, elemental analysis (Table 1) indicates that while the amount of organic surfactant is dramatically reduced, there are still surfactant molecules trapped in the nanorolls even though the *d*-spacing decreases from roughly 3.0 nm to 1.0 nm. In this case, the orientation of these organic molecules must change from perpendicular to parallel to the wall surface. The radius of surfactant molecules (considered as cylindrical shape) is comparable to that of the hydrated sodium ions. The interaction between the organic molecules and hydroxyl groups on the surface of the walls is only van der Waals' interaction (except the head group, which makes an ion pair). This should be an overall weaker electrostatic interaction than that found between the negative oxide walls and positive sodium ions. As a result, despite the presence of some surfactant, the alkali-vanadia interaction is likely to dominate the layered structure of the material. This agrees with previous results which show that nanorolls exchanged with different cations have slightly different *d*-spacings.[9,15,17,18] This is also the probable reason why after sodium exchange, the (10) peaks of the well-ordered and defect-rich nanorolls appear at same position—both are determined mostly by the electrostatic interaction between the sodium ions and the walls. We note that while more than 80 % of the surfactant is lost in both samples, a 10 % greater fraction of the surfactant remains in the well-ordered materials. These organic molecules, together with the sodium ions, serve as spacers between the walls.

2.3. Electrochemical Studies on Ion-Exchanged Nanorolls

The well-ordered ion-exchanged (Na^+, K^+, and Ca^{2+}) vanadia nanorolls have been tested as cathode materials.[17,18] It was found that their capacity is around 200 mA h g^{-1}, which is less than the theoretical value of 240 mA h g^{-1}. However, electrochemical properties, especially of nanoscale materials, are known to be structurally dependent. Thus, we expect that the electrochemical properties of the well-ordered and defect-rich nanorolls may be quite different from one another. In Figure 5, we show the cyclic voltammograms of the sodium-exchanged, well-ordered, and defect-rich vanadia nanorolls. In these experiments, as we sweep the voltage between 4.0 V and 1.5 V, the well-ordered sodium-exchanged nanorolls show several oxidation and reduction peaks (Fig. 5a). Similar results have been reported previously for lithium intercalated samples.[9] This behavior is similar to crystalline orthorhombic vanadium oxide compounds with multiple oxidation–reduction couples and indicates structural transformations from the α–phase to the ε, δ, γ, and ω-phases.[20] Despite these phase changes, however, the basic nanoroll structure is preserved upon electrochemical cycling, as shown in Figure 4d, which presents a TEM image of a nanoroll recovered after charge–discharge cycling.

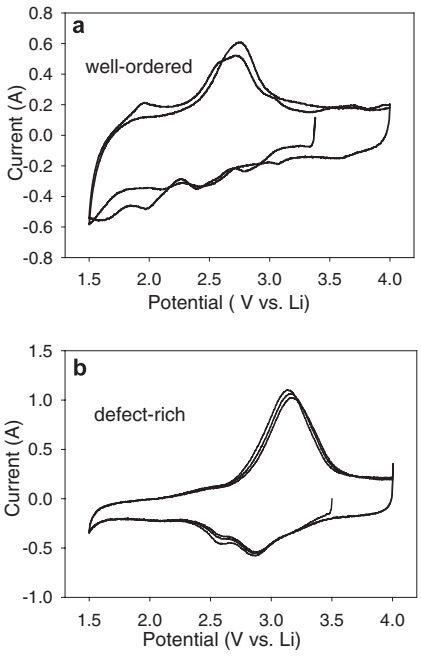

Figure 5. Cyclic voltammograms for Na-exchanged vanadia nanorolls (30 min exchange time) a) well-ordered vanadium oxide nanorolls, and b) defect-rich nanorolls. The well-ordered material shows many steps in the CV curves, similar to crystalline layered vanadates. By contrast, the CV curves for the defect-rich nanorolls are quite similar to sol–gel prepared vanadia.

The defect-rich nanorolls, by contrast, exhibit only one prominent reduction peak at 2.8 V with a shoulder at ~2.6 V. This behavior is similar to that observed in vanadium oxide materials prepared via the sol–gel method.[5] The peak in the defect-rich samples is reversible as no change is observed over several cycles. In contrast, the voltammograms of the well-ordered nanorolls change substantially as cycling continues. It is interesting to note that the potential for the oxidation peak of the defect-rich nanorolls is shifted toward more positive values compared to that of well-ordered nanorolls. More detailed voltammetry studies are necessary to understand why the difference in local order leads to the shift in potential.

The specific capacity of vanadium nanorolls can be affected by many factors. In Figure 6a, we demonstrate how the ion-exchange time affects the capacity of the defect-rich nanorolls. Here we show three samples of defect-rich nanorolls treated for different ion-exchange times: 10 min, 30 min, and 3 h. The XRD patterns of these three sodium nanoroll materials are the same, indicating that these nanorolls are structurally identical. Thermogravimetric analysis (TGA) analysis of these materials, however, indicates a steady decrease in residual organic content (from 8 wt.-% down to 5 wt.-%) as the ion exchange time is increased from 10 min to 3 h, indicating that increase ion exchange time results in more complete surfactant removal. All three nanorolls show an increase in specific capacity after the

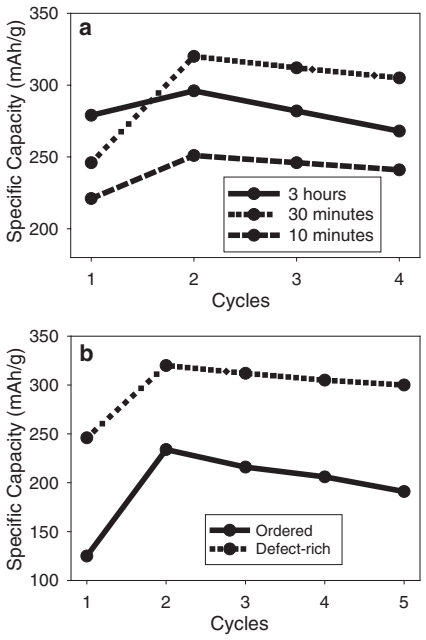

Figure 6. Specific capacity for various vanadium oxide nanoroll samples. In a) the effect of ion exchange time for defect-rich nanorolls is shown. The amount of residual surfactant remaining in the nanorolls appears to have a significant effect on the electrochemical behavior. A larger difference, however, is found when comparing defect-rich and well-ordered nanorolls, which is shown in (b). Both samples were ion-exchanged for 30 min. The defect-rich nanorolls exhibit both higher capacity and better cycle lifetimes.

first charge–discharge cycle, and then a small decrease as cycling continues. Among the three materials, the 30 min sodium-exchanged sample exhibits the highest specific capacity and the slowest rate of capacity decrease with cycling.

The differences in specific capacity with ion-exchange time are likely directly related to the amount of residual organic surfactant trapped inside the nanorolls after ion-exchange. The shortest exchange time leaves more organic molecules between the layers which consequently block access to sites on the vanadium oxide layer that lithium ions would occupy; as a result, this material has the lowest capacity in all cases. The long-exchange time leaves fewer surfactant molecules inside the nanorolls, and thus the 3 h sample has the highest capacity at the first cycle. When the lithium ions are pulled out, however, there are not enough surfactant molecules remaining between the layers to serve as spacers. Thus, some of the electrochemically inserted lithium ions remain in the structure. This lowers the reversible capacity for lithium and decreases the number of available sites for lithium ions to occupy. The 3 h sample thus shows the steepest decrease in capacity upon cycling. The specific capacity of the 30 min ion-exchange nanorolls shows a relatively larger increase in the second cycle with a gradual decrease in capacity on cycling, indicating that the amount of surfactant molecules and their distribution in the nanorolls are most ideal for this sample. The results clearly show that residual surfactant content can dramatically affect the electrochemical performance of these nanorolls.

While surfactant content is important, our results indicate that the atomic and nanometer-scale structure can have an even larger effect on the specific capacity of these nanorolls. In Figure 6b, we present data which tracks the lithium capacities of well-ordered and defect-rich nanorolls, both obtained after the optimal 30 min sodium exchange period. In both materials, the trends in capacity variation with cycling are similar: the capacity reaches its maximum at the second cycle and then decreases as cycling continues. At every point, however, the specific capacity of the defect-rich nanorolls is substantially higher than the corresponding value for the well-ordered material. We note that the data for the well-ordered material agrees well with previous publications which showed a specific capacity for well-ordered sodium-exchanged nanorolls of around 200 mA h g^{-1} within the electrochemical window from 1.8 V to 3.5 V. In addition, this value is in the vicinity of the theoretical value of 240 mA h g^{-1}.[17,18] The defect-rich nanorolls achieve specific capacities well above 300 mA h g^{-1}, marking a significant advance for this material. We also find that the decrease in capacity of the defect-rich nanorolls upon cycling is much slower than the decrease found in well-ordered nanorolls.

The maximum specific capacity that these nanorolls can offer should be approximately the same for both nanoroll types and is given by the following reaction:

$$V_2O_5 + n\,Li^+ + n\,e^- \rightarrow Li_nV_2O_5 \quad (1)$$

Such theoretical capacities (~140 mA h g^{-1}, $n = 1$; ~276 mA h g^{-1}, $n = 2$) are seldom observed, however, since the intercalated phase often has a different structure from the starting material.[31] This is certainly the case for many of the classic layered transition metal oxides that have been studied extensively as cathode materials.[1,19,20] In the nanoroll materials, however, a variety of factors can combine to lead to better accessibility and higher specific capacity.

As discussed above and shown in Table 1, elemental analysis indicates that the amount of surfactant trapped in the well-ordered nanorolls is about 10 % higher than that left in the defect-rich material. These surfactant molecules can reduce the specific capacity in two ways: they not only reduce the available surface area for redox reactions, but they can also form aggregates which may block accessibility of the lithium ions to sites on the vanadium oxide layers. On the other hand, in the defect-rich nanoroll case, even though almost as much surface area is covered by surfactant molecules, the intercalation-deintercalation of lithium ions into and out of the nanorolls can be facilitated by the cracks and exfoliations in the walls. Under this circumstance, the areas surrounded by surfactant molecules that are not accessible to lithium ions in the case of well-ordered nanorolls become active sites for electrochemical reactions. Thus, the only surface areas not accessible to lithium ions are those areas actively covered by surfactant molecules. While this should decrease the theoretical capacity by a small amount, our results from ion-exchange time experiments indicate that a certain amount of surfactant is needed to serve as spacers that prevent the collapse of the gallery spacing between the layers upon electrochemical cycling. We thus speculate that

ADVANCED FUNCTIONAL MATERIALS

the increased accessibility from the cracks should increase the specific capacity in the defect-rich rolls, but more importantly, it should slow the rate of capacity decrease upon cycling—a result that is clearly observed in Figure 6b.

It is likely that the high specific capacity of the defect-rich vanadia nanorolls is also partially due to its local structure. It is now well established that vanadia based materials prepared using sol–gel chemistry can show specific capacities that are significantly higher than related crystalline layered materials.[1,6] In fact, materials have even been produced that show higher than theoretical capacities (i.e., greater than one alkali ion per V_2O_5 unit).[5,6,32,33] This result has been explained by additional cation association with defect sites in the partially disordered vanadia layers and perhaps with some capacitive-like surface charging associated with the nanoscale structure of sol–gel prepared materials.[5–7,34] Figure 5 shows clearly that the defect-rich nanorolls behave electrochemically more like sol–gel vanadia than crystalline layered phases, and so the increased capacity is not surprising. The highest capacity (340 mA h g^{-1}) from our experiments is much greater than the theoretical value ~140 ($n = 1$) or 276 mA h g^{-1} ($n = 2$) of pure V_2O_5.

3. Conclusion

In this study, we have demonstrated the relationship between the nanoscale structure and the electrochemical properties of vanadium oxide nanorolls. Under different synthetic conditions, these nanorolls adopt similar scroll-like structures with different *d*-spacings. The atomic and nanoscale structure of these materials differ in a variety of important ways. Some samples are highly ordered near-perfect rolls, while others have cracks in the walls and regions of large interlayer spacing. This structural difference arises from different ratios of V^{4+}/V^{5+} in the nanoroll walls. When less V^{4+} is present during the synthesis, fewer surfactant template molecules associate with the vanadia layers, resulting in a more defected structure.

Interestingly, the electrochemical properties of the well-ordered and defect-rich nanorolls are quite different. The well-ordered nanorolls behave similarly to classic crystalline vanadium oxides, while the defect-rich materials behave more closely to sol–gel vanadium oxides, which are only partly crystalline on the atomic scale. The combination of nanoscale and atomic scale disorder appears to produce the highly desirable combination of increased specific capacity, and better cyclability. We propose that the increased capacity is associated with additional redox sites that result from the atomic-scale disorder. The better cycle lifetimes are associated with increased accessibility of alkali ions to the gallery regions between the layers because of the cracks and exfoliations in the defect-rich nanotubes.

The results suggest that perfectly ordered structures, while aesthetically appealing, may not be the most optimal structures for many electrochemical applications. The ion diffusion problems associated with highly ordered phases may be a permanent limitation.[35] On the other hand, the complete disorder and high porosity of sol–gel materials can be a disadvantage for some applications. The defect-rich vanadia nanorolls presented here represent a novel compromise. They combine a highly accessible nanoscale architecture with atomic-scale disorder that leads to high capacity. Moreover, the fact that the material is composed of individual, suspendable units means that these materials may be aligned and organized by a range of new microfluidics methods.[22,36–38] Such high capacity colloidal cathode materials may find exciting applications in the next generation of batteries.[39]

4. Experimental

Chemicals and Instruments: Vanadium triisopropoxide oxide was purchased from Gelest (USA), dodecylamine and sodium hexafluorophosphate were purchased from Aldrich. All were used without further purification. Absolute ethanol and 2-propanol were obtained from EM. $LiClO_4$ (99.9 %, Aldrich) was dried under vacuum at 140 °C for several hours before use. Lithium foil (99.99 %, Alfa-Aesa) was cleaned by surface abrasion.

Low-angle X-ray diffraction data were collected using a custom built diffractometer consisting of a Rigaku UltreX18 rotating anode X-ray source (Mo Kα, $\lambda = 0.701$ Å) equipped with a Roper Scientific X-ray charge-coupled device (CCD) camera. High-angle X-ray diffraction patterns were taken on a home built X-ray powder diffractometer (Chemistry Department, UCLA) producing copper Kα radiation ($\lambda = 1.54$ Å). Despite the fact that XRD data was collected using two different X-ray wavelengths, for simplicity, all data in this manuscript is presented as 2θ relative to Cu Kα. X-ray photoelectron spectroscopy (XPS) experiments were performed using a VG Science 220i-XL ESCAlab spectrometer with a Mg Kα source ($h\nu = 1253.6$ eV) and an energy resolution of 0.2 eV. The pressure in the analysis chamber during the measurement was maintained at ~10^{-8} Pa. The powder samples were pressed onto indium foil for analysis. Elemental analysis was performed by Desert Analytical Laboratory, Tucson, Arizona. An Arbin BT4 multichannel potentiostat was used for all electrochemical studies. Residual water content was analyzed by thermogravimetric analysis (TGA) using a Perkin-Elmer Pyris Diamond TG/DTA. Structural characterization through transmission electron microscopy (TEM) made use of a JEOL 2000 electron microscope. TEM samples were prepared by dispersing the nanorolls in absolute ethanol by sonication for ~4 h. Solutions were then dropped onto silicon monoxide coated TEM grids.

Experimental Procedures: In these experiments, we use modifications of the synthetic method reported by Nesper and co-workers to produce our vanadia nanorolls [8,9]. In a typical reaction for well-ordered nanorolls, vanadium triisopropoxide oxide (3.0 g) and dodecylamine (1.9 g) were dissolved in 10.0 mL ethanol (2:1 molar ratio). After stirring for 1 h, de-ionized water (10.0 mL) was added dropwise to the light orange colored solution. The water serves both to hydrolyze the vanadium triisopropoxide oxide and to convert the dodecylamine to dodecylammonium, which is a surfactant. The orange–red precipitate that formed was stirred for another few hours, followed by aging for a week at room temperature. The orange–red solid was isolated by filtration and washed well with water. The isolated composite was then loaded into a 25 mL Parr autoclave vessel with 10.0 mL water and 5.0 mL 2-propanol, which serves as a mild reducing agent. The reaction was allowed to proceed for one week at 180 °C . The defect-rich vanadium oxide nanorolls were prepared similarly to the well-ordered ones except that in the hydrothermal step, the amount of the orange–red composite material was doubled while the solvent volumes were held constant. As a result, the relative amount of reducing agent (2-propanol) was decreased in this synthesis. The black solids obtained from each reaction (well-ordered and defect-rich nanorolls) were collected by filtration and washed thoroughly with de-ionized water and ethanol.

Ion-exchange reactions were carried out at room temperature under vigorous stirring. Sodium hexafluorophosphate and vanadium oxide

nanorolls were mixed at a 4:1 molar ratio in a water/ethanol solution (2.0 mL water + 10.0 mL ethanol).

In the electrochemical experiments, the working electrode was prepared by dip-coating a stainless steel mesh into an ethanol solution containing sodium-exchanged vanadium oxide nanorolls, Ketjen Black, and poly(vinylidene fluoride) (PVDF) (75.0:15.0:10.0 mass ratio). The resulting electrode was heated at 130 °C under vacuum to remove the adsorbed solvents and water. TGA analysis of materials after this heat treatment indicated that the residual water content was quite low (< 0.5 mol) and was nearly identical for each type of nanoroll. The electrode mass was typically ~ 3.0 mg. Electrolytes employed include 1 M $LiClO_4$ in a 1:1 (v/v) mixture of dimethyl carbonate (DMC) and ethylene carbonate (EC) or DMC alone. The cyclic voltammetry (CV) experiments were carried out using a three-electrode cell with the dried vanadium nanorolls/stainless steel mesh as the working electrode and lithium foil as the counter and reference electrodes. The voltage was swept at a rate of 1 mV s^{-1} between 1.5–4.0 V versus Li^+/Li. For galvanostatic experiments, the electrodes were discharged/charged at a rate of ± 60.0 mA g^{-1} between 1.5–4.0 V versus Li^+/Li. All electrochemical experiments were performed in an argon atmosphere glove box.

Received: February 13, 2004
Final version: June 21, 2004

[1] J.-M. Tarascon, M. Armand, *Nature* **2001**, *414*, 359.
[2] P. Poizot, S. Laruelle, S. Grugeon, L. Dupont, J.- M. Tarascon, *Nature* **2000**, *407*, 496.
[3] P. Poizot, S. Laruelle, S. Grugeon, L. Dupont, J.-M. Tarascon, *J. Power Souces* **2001**, *97–98*, 235.
[4] D. Larcher, C. Masquelier, D. Bonnin, Y. Chabre, V. Masson, J.-B. Leriche, J.-M. Tarascon, *J. Electrochem. Soc.* **2003**, *150*, A133.
[5] W. Dong, D. R. Rolison, B. Dunn, *Electrochem. Solid-State Lett.* **2000**, *3*, 457.
[6] D. R. Rolison, B. Dunn, *J. Mater. Chem.* **2001**, *11*, 963.
[7] W. Dong, J. Sakamoto, B. Dunn, *Sci. Technol. Adv. Mater*. **2003**, *4*, 3.
[8] M. E. Spahr, P. Bitterli, R. Nesper, M. Muller, F. Krumeich, H. U. Nissen, *Angew. Chem. Int. Ed.* **1998**, *37*, 1263.
[9] M. E. Spahr, P. Stoschitzki-Bitterli, R. Nesper, O. Haas, P. Novak, *J. Electrochem. Soc.* **1999**, *146*, 2780.
[10] M. Niederberger, H. Muhr, F. Krumeich, F. Bieri, D. Guenther, R. Nesper, *Chem. Mater.* **2000**, *12*, 1995.
[11] D. M. Antonelli, A. Nakahira, J. Y. Ying, *Inorg. Chem.* **1996**, *35*, 3126.
[12] D. M. Antonelli, J. Y. Ying, *Angew. Chem. Int. Ed. Engl.* **1996**, *35*, 426.
[13] J. Y. Ying, C. P. Mehnert, M. S. Wong, *Angew. Chem. Int. Ed.* **1999**, *38*, 56.
[14] T. Sun, J. Y. Ying, *Nature* **1997**, *389*, 704.
[15] J. M. Reinoso, H.-J. Muhr, F. Krumeich, F. Bieri, R. Nesper, *Helv. Chim. Acta* **2000**, *83*, 1724.
[16] G. R. Patzke, F. Krumeich, R. Nesper, *Angew. Chem. Int. Ed.* **2002**, *41*, 2446.
[17] S. Nordlinder, K. Edstrom, T. Gustaffson, *Electrochem. Solid-State Lett.* **2001**, *4*, A129.
[18] S. Nordlinder, J. Lindgren, T. Gustaffson, K. Edstrom, *J. Electrochem. Soc.* **2003**, *150*, E280.
[19] M. M. Thackeray, *Prog. Solid State Chem.* **1997**, *25*, 1.
[20] M. Winter, J. O. Besenhard, M. E. Spahr, P. Novak, *Adv. Mater*. **1998**, *10*, 725.
[21] J. Jamnik, J. Maier, *Phys. Chem. Chem. Phys.* **2003**, *5*, 5215.
[22] H.-J. Muhr, F. Krumeich, U. P. Schönholzer, F. Bieri, M. Niederberger, L. J. Gauckler, R. Nesper, *Adv. Mater.* **2000**, *12*, 231.
[23] F. Krumeich, H.-J. Muhr, M. Niederberger, F. Bieri, B. Schnyder, R. Nesper, *J. Am. Chem. Soc.* **1999**, *121*, 8324.
[24] S. Nordlinder, A. Augustsson, T. Schmitt, J. Gou, L. C. Duda, J. Nordgren, T. Gustafsson, K. Edstrom, *Chem. Mater*. **2003**, *15*, 3227.
[25] A. Monnier, F. Schuth, Q. Huo, D. Kumar, D. Margolese, R. S. Maxwell, G. D. Stucky, M. Krishmnamurty, P. Petroff, *Science* **1993**, *261*, 1299.
[26] S. H. Tolbert, C. C. Landry, G. D. Stucky, B. F. Chmelka, P. Norby, J. C. Hanson, A. Monnier, *Chem. Mater.* **2001**, *13*, 2247.
[27] A. F. Gross, V. H. Le, B. L. Kirsch, S. H. Tolbert, *Langmuir* **2001**, *17*, 3496.
[28] A. F. Gross, S. Yang, A. Navrotsky, S. H. Tolbert, *J. Phys. Chem. B* **2003**, *107*, 2709.
[29] A. F. Gross, E. J. Ruiz, S. H. Tolbert, *J. Phys. Chem. B* **2000**, *104,* 5448.
[30] A. F. Gross, V. H. Le, B. L. Kirsch, S. H. Tolbert, *J. Am. Chem. Soc.* **2002**, *124*, 3713.
[31] D. Carlier, I. Saadoune, M. Menetrier, C. Delmas, *J. Electrochem. Soc.* **2002**, *149*, A1310.
[32] D. B. Le, S. Passerini, A. L. Tipton, B. B. Owens, W. H. Smyrl, *J. Electrochem. Soc.* **1995**, *142*, L102.
[33] D. B. Le, S. Passerini, J. Guo, J. Ressler, B. B. Owens, W. H. Smyrl, *J. Electrochem. Soc.* **1996**, *143*, 2099.
[34] K. E. Swider-Lyons, C. T. Love, D. R. Rolison, *Solid State Ionics* **2002**, *152*, 99.
[35] J. V. Ryan, A. D. Berry, M. L. Anderson, J. W. Long, R. M. Stroud, V. M. Cepak, V. M. Browning, D. R. Rolison, C. I. Merzbacher, *Nature* **2000**, *406*, 169.
[36] B. H. Fishbine, *Fullerene Sci. Technol.* **1996**, *4*, 87.
[37] B. J. Hinds, N. Chopra, T. Rantell, R. Andrews, V. Gavalas, L. G. Bachas, *Science* **2004**, *303*, 62.
[38] Y. Xiong, Y. Xie, S. W. Chen, Z. Q. Li, *Chem. Eur. J.* **2003**, *9*, 4991.
[39] R. W. Hart, H. S. White, B. Dunn, D. R. Rolison, *Electrochem. Commun.* **2003**, *5*, 120.

